Available online at www.sciencedirect.com
SCIENCE DIRECT
International Journal of Heat and Fluid Flow 27 (2006) 267–278
International Journal of HEAT AND FLUID FLOW
www.elsevier.com/locate/ijhff

Nonlinear stochastic estimation of wall models for LES

M. Abel [a,*], D. Stojković [b], M. Breuer [b]

[a] Institut für Physik, Universität Potsdam, Am Neuen Palais 10, Postfach 601553, D-14415 Potsdam, Germany
[b] Lehrstuhl für Strömungsmechanik, Universität Erlangen-Nürnberg, Cauerstr. 4, D-91058 Erlangen, Germany

Received 20 October 2004; received in revised form 15 September 2005; accepted 8 October 2005
Available online 19 December 2005

Abstract

A key technology for large eddy simulation (LES) of complex flows is an appropriate wall modeling strategy. In this paper we apply for the first time a fully nonparametric procedure for the estimation of generalized additive models (GAM) by conditional statistics. As a database, we use DNS and wall-resolved LES data of plane channel flow for Reynolds numbers, $Re = 2800$, 4000 (DNS) and 10,935, 22,776 (LES). The statistical method applied is a quantitative tool for the identification of important model terms, allowing for an identification of some of the near-wall physics. The results are given as nonparametric functions which cannot be attained by other methods. We investigated a generalized model which includes Schumann's and Piomelli et al.'s model. A strong influence of the pressure gradient in the viscous sublayer is found; for larger wall distances the spanwise pressure gradient even dominates the $\tau_{w,zy}$ component. The first a posteriori LES results are given.

Keywords: Large eddy simulation; Nonlinear data analysis; Computational fluid dynamics; Wall models

1. Introduction

Large eddy simulation (LES) is widely considered as a promising tool for the numerical prediction of transitional and turbulent flows. One of the most urgent problems in the development of LES is the treatment of the near-wall region. There, an exclusively large number of grid points, comparable to direct numerical simulation (DNS), is needed to resolve the flow with classical no-slip and impermeability boundary conditions. The currently available subgrid scale (SGS) models are not able to capture the flow dynamics in the near-wall region with the desired accuracy.

A wall model typically reproduces the logarithmic law of the wall encountered in boundary layers without or with mild pressure gradients, hence the first-order statistics are resolved. Higher-order statistics are either not resolved or included by heuristic assumptions. Difficulties to build a reasonable wall model concern the filter width of LES which should decrease close to the wall, the strong inhomogeneity and anisotropy of near-wall turbulence and lacking theory about the statistics of the involved quantities close to the wall. The filtering problem has been discussed in the literature (Ghosal and Moin, 1995; Vasilyev et al., 1998). It is agreed that typically too large filter widths are applied to resolve the local turbulent small-scales. Statistical approaches fail in the wall region due to the entanglement of the physical processes. Some attempts aim at using symmetry decomposition techniques to obtain local scaling laws in the wall region or similarity laws (Benzi et al., 2002; Gualtieri et al., 2002). Investigations on the change of structure functions with the wall-normal coordinate show that an understanding of intermittency and coherent structures is very important (Toschi et al., 1999).

A tool to obtain information about dependencies of flow quantities is the estimation of conditional statistics on the basis of experimental or numerical data (Adrian, 1979; Langford and Moser, 1999). High-dimensional nonadditive and nonlinear models are hard to interpret and require a huge number of observations for good estimation. Models of algebraic character are limited to second-order (Adrian et al., 1989; Nicoud et al., 2001), usually linear

* Corresponding author.
E-mail address: markus@stat.physik.uni-potsdam.de (M. Abel).

0142-727X/$ - see front matter © 2005 Elsevier Inc. All rights reserved.
doi:10.1016/j.ijheatfluidflow.2005.10.011

stochastic estimation (LSE) being used. This might be misleading if the relations involved are not of quadratic order or not of polynomial form. In particular, highly nonlinear models cannot be captured by this way.

To overcome this restriction and for the sake of generality, we propose to use generalized additive models (GAM) and nonlinear, nonparametric regression (Hastie and Tibshirani, 1990) as a generalization of previous techniques. As a result, one obtains equations involving nonparametric, possibly nonlinear functions in a GAM. To indicate the more general character of our approach, we choose to call it nonlinear stochastic estimation (NLSE).

In this publication, we show how to find GAMs by estimating conditional probabilities for use in nonlinear LES wall models. As a data base, we use DNS and wall-resolved LES data for a plane channel flow at low and moderate Reynolds numbers $Re = 2800$, $Re = 4000$ (DNS), and $Re = 10{,}935$, $Re = 22{,}776$ (LES) with $Re = U_b\delta_{Ch}/\nu$, based on the integral scales U_b and δ_{Ch}, the bulk velocity and the channel half-width, respectively. This corresponds to a Re_τ range of $180 \leqslant Re_\tau \leqslant 1056$. We use known models as a priori test cases which are then generalized and extended to a GAM. A quantitative comparison of the results is possible for our analysis. Filtering has not been investigated due to the known problems of the choice of the filter width. However, in principle results for filtered quantities can be constructed from the unfiltered ones. Using instantaneous, unfiltered values, results in terms of correlations look much worse than for filtered ones, because of the integrative effect of the spatial filter. Thus, good results in this article are improved for filtered variables which are applied in LES. At the end of the paper a few a posteriori LES results of the investigated GAM are presented. The prediction is quite acceptable, especially for the $\tau_{w,zy}$ component.

It has to be mentioned that wall models in LES with their coarse resolution of the near-wall region possess numerical and modeling errors. This plays an important role for the overall accuracy of LES predictions (Breuer, 1998, 2002; Moin, 2002). However, within this paper we mainly concentrate on the derivation of appropriate models since this important topic can only be addressed implicitly, based on a posteriori testing of the improved models (see Section 4.3). Additionally, it is clear that wall models can only be applied if a correlation exists between the wall shear stress and the near-wall velocity. Hence, wall functions in general are restricted to y^+ values of the order O(50). Nevertheless, that leads to a decrease in wall-normal grid resolution of two orders of magnitude compared with the no-slip boundary condition and additionally allows to increase the time step size. Thus wall functions are able to substantially reduce the computational costs of LES as will be particularized below.

In general, the LES technique is based on the idea that only the large scales are computed directly which allows to use a coarser grid compared to the resolution required for DNS (Breuer, 2002; Moin, 2002; Pope, 2000). The resulting subgrid scale contributions have to be modeled. The procedure is formulated by the filtered Navier–Stokes equations here given for an incompressible fluid

$$\partial_j \overline{u}_j = 0, \tag{1}$$

$$\partial_t \overline{u}_i + \partial_j(\overline{u}_j\overline{u}_i) = \frac{1}{Re}\partial_{jj}\overline{u}_i - \partial_i\overline{p} - \partial_j\tau_{ij}. \tag{2}$$

The quantity τ_{ij} represents the subgrid scale stress tensor, $\overline{u}, \overline{v}$, $\overline{w}$, and $\overline{p}$ denote the filtered streamwise, wall-normal and spanwise velocity components, and the pressure. The respective coordinates are x, y, and z. The summation convention is used.

The quality of LES results strongly depends on the quality of the subgrid scale model for τ_{ij}. It turned out that reasonable models can be developed for the bulk flow, where the assumption of nearly isotropic turbulence at least approximately holds. Simulations with a coarse grid yield, however, insufficient results close to solid boundaries where the flow is typically inhomogeneous and anisotropic. Attempts to fully resolve the near-wall region lead to very expensive runs because the largest part of the simulation is occupied with the near-wall region. Piomelli and Balaras (2002) estimated the computational costs of a wall-resolved LES to scale as $Re^{2.4}$. Hence appropriate wall models reducing the computational costs to scale as $Re^{0.5}$ are urgently needed to avoid the expensive DNS-like resolution for the near-wall region (see the review by Piomelli and Balaras (2002)).

In the following those models are briefly described which are relevant in the further analysis. We focus on the algebraic models by Schumann (1975), Piomelli et al. (1989), the ejection model (Piomelli et al., 1989), and the gradient model. The known models are briefly explained and then generalized. Other modifications of Schumann's model (Balaras et al., 1996; Grötzbach, 1987; Hoffmann and Benocci, 1995; Piomelli et al., 1989; Werner and Wengle, 1993) will not be considered.

The remaining sections of the paper are organized as follows: in the next section, the nonparametric generalization of wall models is explained and some details of the stochastic estimation procedure are given. In Section 3 the generation and pre-processing of the DNS and LES data involved is explained. Finally, the results for the models investigated are presented and discussed in Sections 4 and 5.

2. Nonlinear stochastic estimation and generalized additive models

In this section, we will generalize existing wall functions towards a nonparametric representation. In the approach of Schumann (1975) a phase coincidence of the instantaneous wall shear stress and the tangential velocity component in the first off-the-wall cell is assumed. Combining this assumption with the impermeability condition, the resulting system of equations for a wall parallel to the x-axis reads

$$\tau_{w,xy}(x,z,t) = \frac{\langle \tau_w \rangle}{\langle \overline{u}(Y) \rangle} \overline{u}(x,Y,z,t), \tag{3}$$

$$\tau_{w,yy}(x,z,t) = 0, \tag{4}$$

$$\tau_{w,zy}(x,z,t) = \frac{1}{Re} \frac{\overline{w}(x,Y,z,t)}{Y}, \tag{5}$$

where x, y, z, t denote the streamwise wall-normal, and spanwise coordinates and the time; Y represents the distance of the wall-nearest grid point from the wall and $\langle \cdot \rangle$ denotes time- and space-averaging in homogeneous directions. Implicitly, $\overline{v}$ is set to zero. This model contains no adjustable parameters, but a Y-dependent slope $\langle \tau_w \rangle / \langle \overline{u}(Y) \rangle$. Eq. (3) is linear in $\overline{u}$. However, intermittency and the occurring large fluctuations at larger wall distance suggest that there can exist nonlinear relations of the form $\tau_{w,xy} = f_u(\langle \overline{u}(Y) \rangle)$. In Langford and Moser (1999) this is treated by expanding the function f_u. Up to second-order this yields

$$f_u(\overline{u}) = \mathbf{L}\overline{u} + \overline{u}\mathbf{N}\overline{u} + \cdots. \tag{6}$$

The tensors $\mathbf{L}$ and $\mathbf{N}$ are first and second-order, respectively. Thus this is a *nonlinear, but parametrized* model, restricted to be quadratic. To find the tensors $\mathbf{L}$ and $\mathbf{N}$ by stochastic estimation, one applies standard, *fully linear*, least-squares regression (Teukolsky et al., 1993). The generalized formulation of Schumann's model reads

$$\tau_{w,xy} = f_{u,S}(\overline{u}(Y)), \quad \tau_{w,yy} = 0, \quad \tau_{w,zy} = f_{w,S}(\overline{w}(Y)), \tag{7}$$

where we omitted x, z, and t dependence for better readability. All constants, slopes and other parameters are absorbed into the nonparametric functions $f_{u,S}$ and $f_{w,S}$. For such a model, we can find a nonparametric estimate for the function f_u. This is demonstrated below; but before explaining the estimation procedure, we want to formulate a more general model, which includes Schumann's formulation as a submodel. In Piomelli et al. (1989), a streamwise delay, δ, takes the existence of inclined structures in the near-wall region into account

$$\tau_{w,xy}(x,z,t) = \frac{\langle \tau_w \rangle}{\langle \overline{u}(Y) \rangle} \overline{u}(x+\delta,Y,z,t), \tag{8}$$

$$\tau_{w,yy}(x,z,t) = 0, \tag{9}$$

$$\tau_{w,zy}(x,z,t) = \frac{\langle \tau_w \rangle}{\langle \overline{u}(Y) \rangle} \overline{w}(x+\delta,Y,z,t). \tag{10}$$

The corresponding generalized model differs from Eq. (7) only in the arguments of the velocity components: they are shifted by δ. In order to work with nondimensional quantities, we introduce the following definitions: $\widetilde{\tau}_w = \tau_w / \langle \tau_w \rangle$, $\widetilde{u} = \overline{u} / \langle \overline{u}(Y) \rangle$, $\widetilde{v} = \overline{v} / \langle \overline{u}(Y) \rangle$ and $\widetilde{\partial}_x \widetilde{p} = \overline{\partial_x p} / (\rho \langle \overline{u}(Y) \rangle^2 / \delta_{Ch})$ for the normalized quantities. A similar definition can be applied to the unfiltered values. If no ambiguities exist, we omit the "~"-sign. Consequently, in normalized variables the slope of Schumann's model equals one.

Another set of equations proposed in Piomelli et al. (1989), the ejection boundary condition, correlates the wall-normal velocity with $\tau_{w,xy}$ leading to the *ejection model*

$$\tau_{w,xy}(x,z,t) = \langle \tau_w \rangle - C \overline{u}_\tau \overline{v}(x+\delta,Y,z,t). \tag{11}$$

We can now combine the three presented models (Schumann, Piomelli, ejection) into one generalized, nondimensionalized model

$$\tau_{w,xy}(x,z,t) = f_{u,e}(\overline{u}(\vec{r},t)) + f_{v,e}(\overline{v}(\vec{r},t)), \tag{12}$$

$$\tau_{w,yy}(x,z,t) = 0, \tag{13}$$

$$\tau_{w,zy}(x,z,t) = f_{w,e}(\overline{w}(\vec{r},t)), \tag{14}$$

with $\vec{r} = (x+\delta, Y, z)$. To generalize further, including the previous models, the influence of the local pressure gradients (see Craft et al., 2002) in x- and z-directions are included leading to the "pressure gradient model" (abbreviated by *gradient model*)

$$\tau_{w,xy}(x,z,t) = f_{u,g}(\overline{u}(\vec{r},t)) + f_{v,g}(\overline{v}(\vec{r},t)) + f_{px,g}(\partial_x \overline{p}(\vec{r},t)), \tag{15}$$

$$\tau_{w,yy}(x,z,t) = 0, \tag{16}$$

$$\tau_{w,zy}(x,z,t) = f_{w,g}(\overline{w}(\vec{r},t)) + f_{vz,g}(\overline{v}(\vec{r},t)) + f_{pz,g}(\partial_z \overline{p}(\vec{r},t)). \tag{17}$$

Now, we will refer to nonlinear stochastic estimation and show how to estimate the above additive models, which are generically nonparametric and nonlinear. Technical points are omitted and only the basic principles will be explained. As mentioned above, we work with unfiltered quantities, and consequently the over-bar for averaging does not occur anymore below.

Stochastic estimation has been introduced for the approximation of conditional events in turbulence by Adrian (1979), and Adrian et al. (1989). Recently, the topic has been revived (Langford and Moser, 1999; Meneveau and Katz, 2000; Nicoud et al., 2001; Völker et al., 2002), where in all publications a linear estimation procedure has been used. On the other hand, in statistics conditional expectation values are used in nonparametric analysis involving kernel smoothers, smoothing splines and other techniques (Green and Silverman, 1994; Hastie and Tibshirani, 1990; Silverman, 1996). The use for the modeling of spatio-temporal systems has been proposed in Voss et al. (1998).

We are interested in inferring a dependence of a quantity, say $\tau_w(\vec{r},t)$, on a set of N other quantities, say $u(\vec{r},t), v(\vec{r},t), w(\vec{r},t)$ and $p(\vec{r},t)$ ($N=4$). The data are related by the parameters $\vec{r}$ and t and thus represent a set of points in $N+1$-dimensional space. We first restrict the discussion to a model of two constituents. Generalization to higher model dimensions is considered below.

Given two random variables (τ_w, u)—the data—one wants to test if a model of the type

$$\tau_w(\vec{r},t) = f_u(u(\vec{r},t)) + \epsilon \tag{18}$$

is satisfied, with modeling error ϵ. The function f_u formally needs to be a measurable function. To find an estimate $\widehat{f}_u$ for f_u, the conditional expectation value operator $E(\tau_w|u)$ is used

$$\widehat{f}_u(u) = E(\tau_w|u) = \int P(\tau_w'|u) \tau_w' \, \mathrm{d}\tau_w', \tag{19}$$

where $P(\tau_w'|u)$ denotes the conditional probability, and the condition

$$E\left(\left[\tau_w(\vec{r},t)-\widehat{f}_u(u(\vec{r},t))\right]^2\right)=\min \tag{20}$$

is fulfilled. As in linear estimation techniques the best expression is found in the least-squared sense. It can be shown that this is equivalent to the estimation of the optimal function in the sense of correlation (Rényi, 1959), which will be referred to below. The above formulation follows the outline given in Langford and Moser (1999). In the following, the hat for estimated quantities and the dependence on the parameters $\vec{r}$ and t is omitted, if no ambiguity exists. Numerically, the estimation procedure is realized by kernel methods such as Gaussian weighted averages, running mean (or moving average) filter, or smoothing splines (Hastie and Tibshirani, 1990). To obtain twice differentiable functions, we use a spline smoother. Further processing can lead to a suitable nonlinear function, e.g., in parameterized form. We emphasize that this is *not* the same as parameterizing beforehand and running a linear regression. A nonparametric model can, e.g., yield logarithms, piecewise linear functions or any other measurable function. Obviously, this is excluded, if parameterization is applied before the analysis.

In the case of higher-dimensional models,

$$\tau_w=F(u,v,w,p,\ldots)+\epsilon \tag{21}$$

in principle, one has to estimate the conditional probability $P(\tau_w|u,v,w,p,\ldots)$ (Langford and Moser, 1999). Due to the high dimensionality of the model, a reliable estimation of P requires a prohibitive number of points. Additionally, it is hard to visualize results for dimensions larger than two. With the restriction of a generalized *additive* model (GAM), however, an efficient iteration procedure has been developed to solve the task. Such a GAM has the form

$$\tau_w(\vec{r},t)=f_u(u(\vec{r},t))+f_v(v(\vec{r},t))+f_w(w(\vec{r},t))+\cdots+\epsilon. \tag{22}$$

This is precisely the structure of the wall models (7), (12), and (15). For a GAM, the multi-dimensional minimization procedure is solved numerically with a so-called backfitting algorithm (Hastie and Tibshirani, 1990). One projects in each iteration on a two-dimensional plane and thus avoids the problems arising for higher dimensions. To obtain the required estimate, smoothing is used (Buja et al., 1989). In the following, we will speak loosely of a GAM, even if only two components are involved.

A measure of quality is derived from the residual part ϵ. We write a GAM of $N+1$ variables $\{\tau_w, V_i\}_{i=1,\ldots,N}$ in a general form as

$$\tau_w=\sum_{i=1}^{N} f_i(V_i)+\epsilon, \tag{23}$$

where V_i can be any relevant quantity dependent on $\vec{r}$ and t. The intuitive measure of how good the model represents the data, is the standard deviation $D_\epsilon=\sqrt{\langle[\tau_w-\sum_{i=1}^{N}f_i(V_i)]^2\rangle}$. It ranges from 0 to infinity and depends on the value of τ_w. Normalizing with the variance of τ, $\mathrm{VAR}(\tau_w)$, yields $D_\epsilon \lesseqgtr 1$ to indicate small or large model deficiencies, respectively.

If nonlinear models are considered, it is natural to work with the correlation $C(\zeta,\xi)$ of the two random variables ζ and ξ (Honerkamp, 1994)

$$C[\zeta,\xi]=\frac{\langle(\zeta-\langle\zeta\rangle)(\xi-\langle\xi\rangle)\rangle}{\sqrt{\mathrm{VAR}(\zeta)\mathrm{VAR}(\xi)}}. \tag{24}$$

The correlation C ranges from -1 (anti-correlation) over 0 (complete decorrelation) to 1 (correlation). Mean values are subtracted, and the variances are divided out. Thereby nonlinear effects are more clearly seen. Slopes and constants of linear models such as $\tau_w=\alpha+\beta u$ are estimated, too, if the algorithm is used as an iterative solver for linear regression. For comparison, we study D_ϵ and C for Schumann's model; later on only the correlations are used.

To have an information about the distance from the wall, for which a model is still meaningful, we calculate the correlation $C(Y)$ dependent on the wall-normal distance Y. In the GAM (23), one calculates $C_0=C[\tau_w,\sum_{i=1}^{N}f_i(V_i)]$, where the subscript 0 stands for the lhs. If one projects the error on different coordinates, one calculates analogously $C_j=C[f_j(V_j),\tau_w-\sum_{i=1,i\neq j}^{N}f_i(V_i)]$. This corresponds to the residual part in the projection onto the jth coordinate. The curve $C_j(Y)$ then gives a measure of the importance of the respective function $f_j(V_j)$ for the model. Since a nonparametric form is used, one works with the transforms f_j and not with the variables V_j themselves. For more details, see Abel (2004), and Hastie and Tibshirani (1990).

Given a general wall model such as Eqs. (15)–(17), one can identify the role which each term plays for the wall shear stress, and furthermore pin some region where the deterministic model or some constituents are significant. The different correlations to be calculated are

$$C_0(Y)=C[\tau_{w,xy},f_u+f_v+f_{px}], \tag{25}$$
$$C_1(Y)=C[f_u,\tau_{w,xy}-(f_v+f_{px})], \tag{26}$$
$$C_2(Y)=C[f_v,\tau_{w,xy}-(f_u+f_{px})], \tag{27}$$
$$C_3(Y)=C[f_{px},\tau_{w,xy}-(f_u+f_v)], \tag{28}$$

where the subscript "g" is omitted. For the $\tau_{w,zy}$ component, one calculates the analogous quantities. The model (15)–(17) includes the models (3)–(12) as sub-models. Since the nonparametric analysis identifies the importance of different terms, it is sufficient to analyze this model. The results for a sub-model can then be read from the corresponding curves of the correlations (Abel, 2004). We checked the application of the analysis to the sub-models, and found everything to be consistent.

3. DNS and wall-resolved LES data

The data we used throughout this article have been obtained by DNS and wall-resolved LES predictions using the second-order, finite-volume code *LESOCC* (Breuer,

1998, 2002). Because the nonlinear analysis shall be tested on the best case available, we produced instantaneous and highly-resolved near-wall data for a plane channel flow. For comparison with previous results, we first studied this setup as a "standard" test case.

To investigate the dependence of the results on the Reynolds number Re, we produced DNS data for two Reynolds numbers, $Re = 2800$ and $Re = 4000$. For $Re =$ 10,935 and 22,776, we carried out a wall-resolved LES. Hence a Re_τ-range of $180 \leqslant Re_\tau \leqslant 1056$ is covered. We emphasize that it is convenient to use the LES results for comparison of a posteriori LES simulations with the wall models found by the a priori analysis. This way, one can use exactly the given LES configuration to compare the results obtained.

The geometry of the channel was $L_x/\delta_{Ch} = 6$, $L_y/\delta_{Ch} = 2$ and $L_z/\delta_{Ch} = 3$. The flow was driven by a pressure gradient in streamwise direction which was adjusted during the simulation to guarantee a fixed mass flux. In stream- and spanwise directions periodic boundary conditions are used, whereas at the walls no-slip and impermeability conditions are applied. The dimensionless time step was $\Delta t = 0.0025$. Different Cartesian grids with varying number of grid points and grid stretching in wall-normal direction are used. Table 1 gives an overview of all cases.

For the analysis a sub-domain $\Delta x_{sub} \otimes \Delta y_{sub} \otimes \Delta z_{sub}$ of the entire integration volume is used; e.g., at $Re = 10{,}935$ $\Delta x^+_{sub} = 3500$, $\Delta y^+_{sub} = 580$ and $\Delta z^+_{sub} = 320$. This reduces the amount of data to a size which can be handled on a workstation. The complete data sets of this sub-domain are stored for all instantaneous quantities and made available for the subsequent analysis. Taking the three-dimensional part of the volume, we obtain accurate statistical information, especially with regard to large fluctuations. The problem of errors on the estimates will be discussed below (cf. Fig. 2(b)).

To ensure statistical independence we recorded 125 data sets within a time interval of $t_{stat} = 25$. Consequently, two samples are separated by $\Delta t_{stat} = 0.2$. Longer time intervals would be desirable but lead to huge amount of data not manageable within reasonable time. The problem of intermittency and long tails in the PDFs of velocity increments means that extreme values occur very rarely and thus the corresponding estimates for our models have statistical errors.

For LES one typically considers filtered data. In contrast to this, we base our investigation on instantaneous data. The reason is that we do not want to enter a long, necessary discussion about the asymmetric filtering procedure to be used close to the wall, but focus on the estimation procedure. For some simple filters such as the top-hat filter, one can even conclude the filtered results from the instantaneous ones. In general, a filter raises the value of the correlations, because of its integrative functioning. Thus, for filtered quantities results are better than for the unfiltered quantities presented below; the worst case is shown. We checked different filtering procedures confirming the picture sketched above. In the models described above, mean values such as $\langle \tau_w \rangle$ and $\langle \overline{u} \rangle$ occur. Within an LES prediction both quantities would be part of the solution procedure and determined on-the-fly by averaging the corresponding unsteady values.

4. Results

The goal of a wall model is to relate the wall shear stress τ_w with the fields in the outer flow, using a model in the inner region. To acquaint the reader with the concepts, we first discuss Schumann's generalized model. Then results for the gradient model are considered. In the case of Schumann's model, we compare possible linear models (LSE) with each other and with the nonlinear one (NLSE). In the case of nonlinear models, we plot the resulting nonlinear functions and interpret the results. We have chosen to show most of the details for the wall-resolved LES at $Re = 10{,}935$. If the influence of the Reynolds number is investigated, results for all four data sets are shown.

4.1. Schumann's model

A linear generalization of the model of Schumann (Schumann, 1975) reads

$$\tau_{w,xy}(x,z,t) = \alpha_1 + \beta_1 u(x,Y,z,t) + \epsilon, \tag{29}$$

$$\tau_{w,zy}(x,z,t) = \alpha_3 + \beta_3 w(x,Y,z,t) + \epsilon, \tag{30}$$

with α_1, α_3, β_1, β_3 constants. The equation for $\tau_{w,yy} = 0$ remains unchanged. For the further discussion, we distinguish the following models S1–S4 for the $\tau_{w,xy}$ component:

- S1: the original, linear model of Schumann with fixed slope, $\beta_1 = 1$, $\alpha_1 = 0$,
- S2: a linear model with slope $\beta_1(Y) \neq 1$ ($\alpha_1 = 0$) to be determined by LSE,
- S3: a model with a constant $\alpha_1(Y) \neq 0$ and slope $\beta_1(Y) \neq 0$ (LSE),

Table 1
Summary of grid parameters for the different DNS and wall-resolved LES predictions

Re	n_x	n_y	n_z	Δx^+	Δy^+_{min}	Δz^+	u_τ
2800 (DNS)	120	162	112	8.97	0.176	4.81	0.0630
4000 (DNS)	150	208	120	9.70	0.239	6.08	0.0598
10,935 (LES)	120	162	112	29.69	0.584	15.92	0.0534
22,776 (LES)	150	208	120	42.84	0.420	26.87	0.0464

S4: the nonparametric model (7) with a general function $f_{u,S}(u, Y)$.

To characterize the models, we calculate $D_\epsilon(Y)$ and $C(Y)$. Except for S1, we run a regression analysis on the data, linear in the case of S2 and S3 (LSE), and nonlinear in case of S4 (NLSE). We then compared the results of the models S1–S4. As seen from Eq. (24), models S1–S3 yield exactly the same result for the correlation function $C(y^+)$, because α and β are automatically scaled out (α, β are combinations of means and variances); nonlinear effects are found by comparing $C_{S1-S3}(Y)$ with $C_{S4}(Y)$.

The plot with the comparison of the models S1–S4, for the different Reynolds numbers investigated is displayed in Fig. 1. In Fig. 1(a) the error, $\epsilon(y^+)$, is plotted. With increasing Re the error grows reflecting intermittent fluctuations which increase with the Reynolds number. The inset shows a comparison for the different models S1–S4. As expected, S1 has the largest error and S4 the smallest one. The relative difference is about 10% which is not very large. In Fig. 1(b) the correlations, $C(y^+)$, are shown for different Re with the inset displaying the differences between LSE and NLSE. In contrast to the error, the correlations grow with increasing Re, which shows that the normalization with the variance is important in this case. The relative change with Reynolds number becomes smaller indicating a convergence towards one high-Re curve. If different models are compared, one finds that NLSE yields only a slightly higher correlation than LSE which is consistent with the error and suggests linear modeling. Hence, error and correlations behave similar for all Re in the viscous subrange. For larger wall-normal distances y^+ the correlations decay slower with increasing Re, and the error correspondingly grows. The correlations decay relatively fast between $y^+ = 40$ and $y^+ = 100$ to a value of $C = 0.1$.

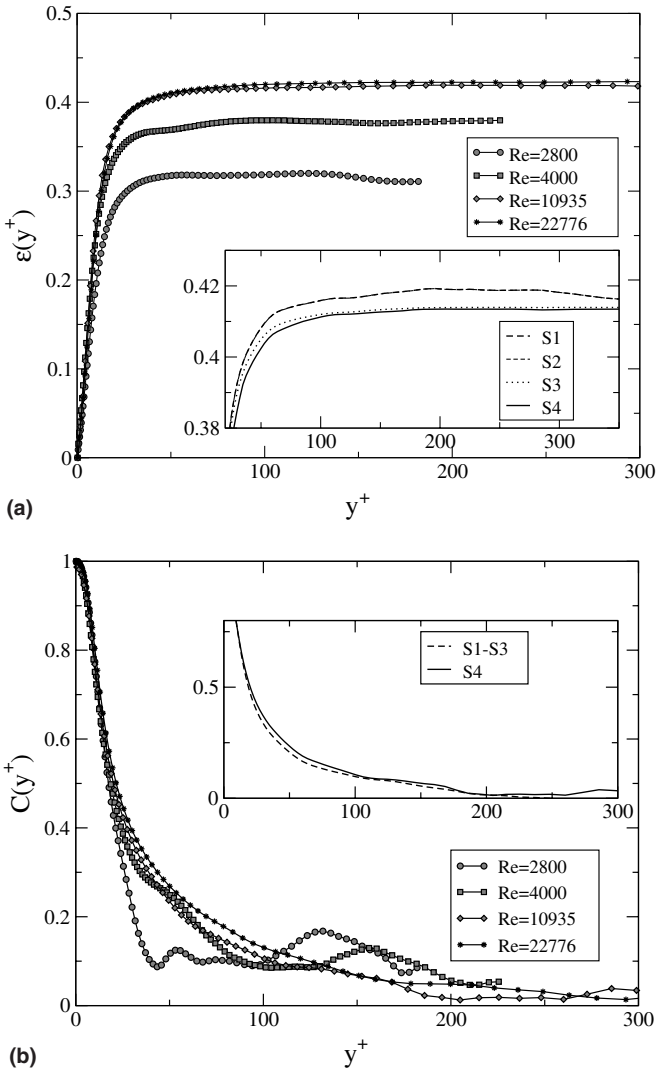

Fig. 1. (a) Error estimates $\epsilon(y^+)$ and (b) correlations $C_0(y^+)$ for LSE and NLSE of Schumann's model. The graphs show comparison of $Re = 2800$ (●), $Re = 4000$ (■), $Re = 10{,}935$ (◊), and $Re = 22{,}776$ (*); the inset shows the comparison of results for different models ($Re = 10{,}935$).

For model S3, the coefficient α_1 increases monotonously over a range $0 < y^+ < y^+_{max}$ from 0 to a maximum value and decreases again for large y^+. The location of the maximum varies with the Reynolds number, but is in the range of very small correlation. The slope β_1 decreases from 1 to a minimum located approximately at the location of the maximum of α_1. For implementation in LES, one has to take these values, if a linear model is considered. This can be seen as one result of our investigations and is consistent with earlier observations for coherent structures (Jimenèz and Siemens, 2001). It is known that large a priori errors do not necessarily lead to bad a posteriori results (Ferziger, 1996; Langford and Moser, 1999).

The corresponding nonparametric functions $f(u(y^+))$ are displayed in Fig. 2(a) for $Re = 10{,}935$. For a clearer presentation an offset is added to each function. From small to large values of y^+ the functions are first linear, as expected, then a bend at the end of the accessible values for u is observed, turning the function to be more nonlinear. Finally the functions are constant (equal to the mean value $\langle u(y^+)\rangle$) with fluctuations in the tails. This is due to increasing loss of information for increasing wall distances once the viscous sublayer is left. Decorrelation is first observed at the high and low velocities, where, however, the statistics for the estimation of the function is not very accurate.

This is recognized in Fig. 2(b), where the results are explained by a study of one particular graph, for $f(u(y^+ = 30))$. The function is plotted on top of the a part (2000 points) of the scatter, $f(u) + \epsilon(u)$; together with the distribution of the u-values. Clearly, the part with the highest probability shows quite little scatter, and the residual part aligns with the function quite well. On the other hand, in regions with low probability, one obtains enormous scatter which finally yields the bad correlations seen in Fig. 1. The low probability region in the PDF represents exactly the part where intermittency effects strongly influence the statistics. The large scatter of the residuals can be explained by the highly intermittent flow in the near-wall region. So,

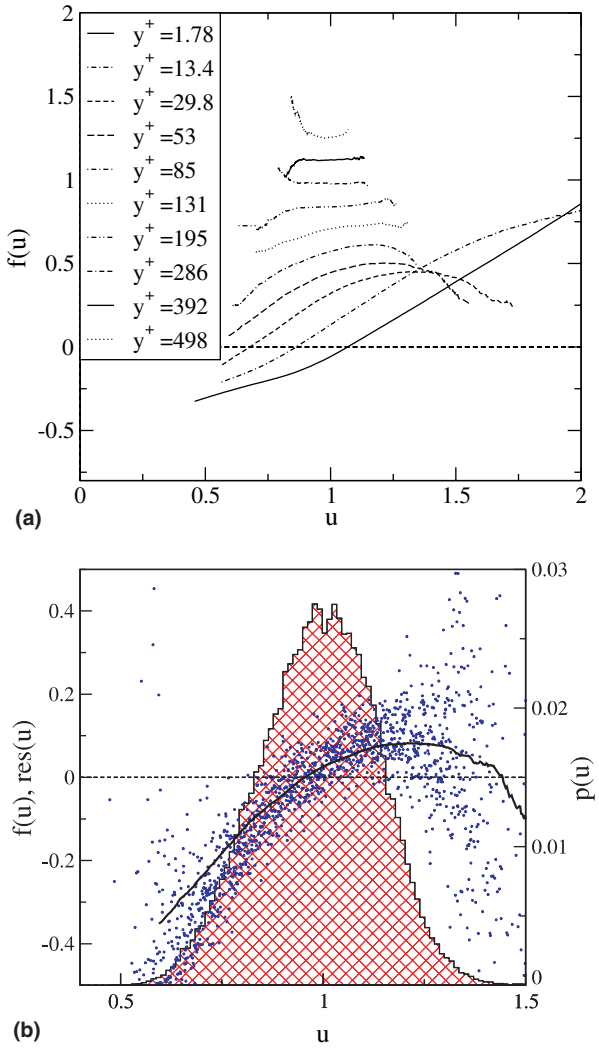

Fig. 2. Optimal functions for $Re = 10{,}935$ from NLSE: (a) collection of functions for various distances y^+. An arbitrary offset (multiples of 0.14) is added to each function for better visualization. Without the offset all functions overlap and cannot be well distinguished. (b) Case study for $y^+ = 30$. The grey, cross-shaded region indicates the distribution of u-values, $p(u)$; the grey crosses mark the residual scatter, $res(u)$.

the optimal functions obtained represent a good model in some core region. In the tails of the distribution, i.e., for low and high velocities, however, one needs even longer runs to ensure statistical reliability and should include higher moments of the PDF.

These considerations explain as well why there is no big difference between LSE and NLSE: those rare events possess almost no statistical weight in usual linear least-squares procedures. In contrast to this, NLSE gives for these regions separate estimates. It is the right tool to analyze functional dependencies for intermittent processes where rare events play a role. In any case, it is crucial not to apply blindly the fitted results in an LES (a posteriori), rather one has to interpret the results on the basis of careful inspection of the functions with their residuals and distributions of values.

We resume at this point by noting that a wall model of Schumann's type, although generalized, should be linear with varying slope β and nonzero offset α for values of about $y^+ \lesssim 20$; then a nonlinear model should be used in the range $20 \lesssim y^+$. With respect to the Reynolds number dependence, a convergence towards stable results is found. For small y^+ the functions coincide, for large distances, differences are found, corresponding to the different correlations observed.

4.2. Gradient model

The gradient model (15) is motivated by using two basic velocity components for the xy and zy component of the wall stress tensor plus the respective components of the pressure gradient. The latter represents the deviation from the mean pressure gradient in the channel. The pressure gradients are included with the hope to better capture separated flows (Craft et al., 2002).

With respect to different Reynolds numbers, we observed that correlations and functions show convergence with increasing Reynolds number similar to the above described results. The functions become clearer in shape, even in their tails. This is to our opinion a sign of convergence to a statistically more homogeneous state (within each plane).

4.2.1. The $\tau_{w,xy}$-component

The cumulative result is given in terms of the correlations C_0–C_3, cf. Eqs. (25)–(28). The comparison of the data sets for different Re is shown in Fig. 3(a) as a plot of $C_0(y^+)$. The corresponding delay is plotted in Fig. 3(b). For comparison, the C_0-curve for $Re = 10{,}935$ of Schumann's model is shown. As for Schumann's model, for a fixed y^+, the correlations increase with increasing Re showing convergence to a high-Re curve. The correlation is clearly higher than in Schumann's case, confirming the idea of Piomelli et al. to include a delay δ to take inclined structures into account.

For $Re = 10{,}935$, we show the correlations C_0–C_3 in Fig. 4. From this plot the influence of the different terms can be concluded. The major weight is carried by the u-dependence. The correlation for the v-dependent term increases from zero a maximum at $C_2(y^+ \simeq 15) \simeq 0.5$ to tend to zero monotonously with further increasing y^+. The pressure gradient dependence has a peak value ($C_3 \simeq 0.85$) at $y^+ = 1.77$, i.e., right at the wall to quickly decrease with increasing wall distance. A model should consequently contain a pressure gradient term close the wall, and the wall-normal velocity in a certain region between the viscous sublayer and the log-layer. For $y^+ \simeq 200$, C_1–C_3 are equally low due to large fluctuations. The judgment of the contributions of v and $\partial_x p$ depends on the modelers choice: one can define an "importance criterion" choosing (quite arbitrarily) a value of $C = C_{\text{crit}}$ below which one does not take into account model terms. For example, taking $C_{\text{crit}} = 0.3$ tells that the gradient term

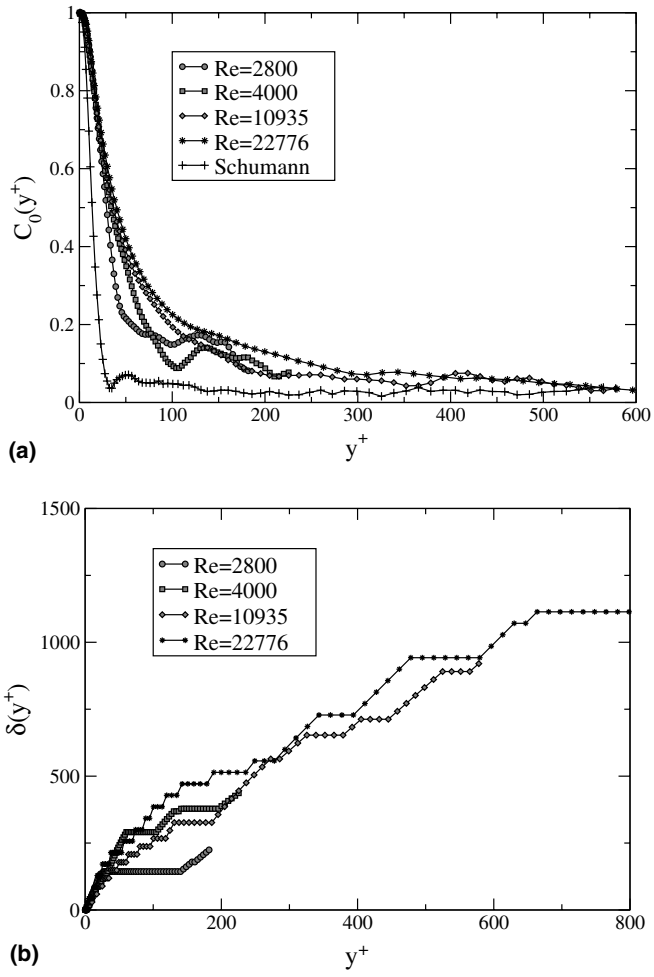

Fig. 3. (a) Correlations $C_0(y^+)$ for the Reynolds numbers investigated. For comparison the curve for Schumann's model at $Re = 10{,}935$ is shown as well (+); (b) corresponding delay in units of x^+.

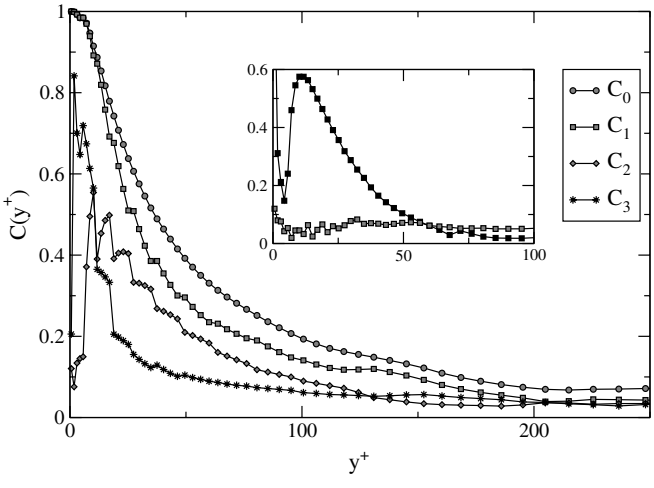

Fig. 4. Correlations C_0, C_1, C_2, and C_3 for the $\tau_{w,xy}$-component at $Re = 10{,}935$. The inset shows correlations C_2 for a set with sweeping events only (■) and ejections only (■), respectively.

can be discarded for $y^+ > 15$ and the term of the wall-normal velocity for $y^+ > 35$. Furthermore, modeling becomes then "useless" for $y^+ > 65$ because $C_0 < C_{\text{crit}} = 0.3$. Note that despite low correlations, a formulation by the average can still make sense. For Fig. 2(b) we discussed the effects of the large fluctuations for different regions of a function—in the center fluctuations are small and thus the relative error, in the tails, due to intermittency fluctuations are large, but the mean is still well defined. These errors do not necessarily worsen a posteriori LES evaluation.

In Fig. 5(a) and (b) the optimal functions f_v and f_{px} are plotted. The function f_u is omitted here since it shows a similar behavior than for the generalized Schumann model (see Fig. 2(a)): linear in the near-wall region to nonlinear and finally constant at large distances. The delay is prolonging the region of linear shape and raises the value of the correlation. The distribution of u-values is evidently the same as shown in Fig. 2(b), such that also here the tails of the functions are strongly influenced by intermittent events and thus must be considered with caution.

The function $f_v(v)$ does contribute in the range $y^+ \lesssim 100$. The corresponding plots show that one can

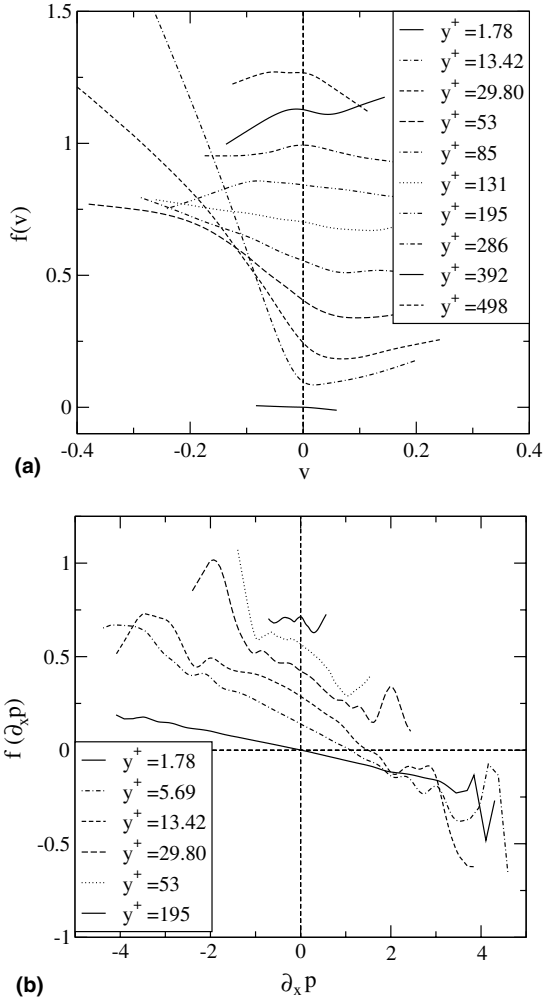

Fig. 5. Collection of functions at different distances y^+. (a) $f_v(v)$ and (b) $f_{px}(\partial_x p)$. The functions for f_u are similar to Fig. 2(a) and thus not shown here. The same offset as in Fig. 2(a) is added for better visualization.

roughly put $f_v = \alpha v$ for $v < v_{\text{crit}}$ and $f_v = 0$ for $v \geqslant v_{\text{crit}}$ with $v_{\text{crit}} = -0.02 \simeq 0$. The slight increase for positive values is due to the spline representation. Analyses have been run for data sets with only sweeping and only ejection events. The corresponding correlations C_2 are shown in the inset of Fig. 4(b); there is no contribution from ejections yielding $C_2 \simeq 0$, and a clearly smoother curve for sweeping events indication their statistical relevance. If an inclined structure consists of a stretched vortex at a certain angle with the wall, our result means that the wall shear stress is determined by the part of the vortex which moves fluid towards the wall.

In Fig. 5(b) the $f_{px}(\partial_x p)$ values close to the wall are plotted. The behavior is linear with a negative slope in the significant region. In the log-layer, where the correlation is vanishing, the function $f_{px}(\partial_x p)$ is vanishing. This function is expected to become important for flows with separation. Thus, it is interesting to see the high influence of the pressure gradient, even though restricted to wall distances unimportant for real LES. Nevertheless, conceptually this issue guides towards a model with a pressure gradient term.

4.2.2. The $\tau_{w,zy}$-component

In this section we show results for the zy-component of the wall shear stress. Details for the functions are only shown for relevant terms. The correlations at $Re = 10{,}935$ are plotted in Fig. 6. We omit comparison for different Re, the overall behavior is similar to the $\tau_{w,xy}$ component.

The correlation C_1, which corresponds to the Schumann component $f_w(w)$ decays quite rapidly (■ in Fig. 6) and for $y^+ \simeq 25$ the spanwise pressure gradient $f_{pz}(\partial_z p)$ dominates. The gradient model yields clearly higher correlations in comparison to Schumann's model (* in Fig. 6). The correlations decay to almost zero within 100 wall units. The wall-normal velocity (represented by C_2) appears only within a few points of the viscous sublayer and thus is unimportant for this component of the stress tensor. Because the results displayed are obtained by wall-resolved LES data, the resolution in x-direction is coarser than for the low-Re cases leading to discrete jumps in the space delay δ also visible in the correlations (at $y^+ = 11$). Only a delay of one spatial resolution step, $\Delta x^+ = 29.7$, is observed in a significant range of C (e.g., $C > 0.1$). The optimal functions are not shown here. In brief, for f_w and f_{pz}, the graphs are slightly nonlinear in the relevant range. Beyond $y^+ = 100$ all functions are negligible similar to f_v for all y^+. It is interesting to note that the pressure gradient plays such a clear and dominant role within the buffer layer up to the log-layer. We cannot give a clear explanation for this behavior.

4.3. A posteriori analysis: first results

For an implementation into an LES code, one can take the output of the nonparametric estimation in terms of B-splines and construct the value of the functions in each point. A more sensible procedure is to try to approximate the function globally, as in the case of f_v, where $f_v = 0$ for $v > v_{\text{crit}}$ and linear else. This way, one disregards the problematic estimation of functions in the tails and obtains quite robust functions for numerical use. A fitting procedure should first be inspired by inspection of the function plots. Then known functional forms such as polynomials or exponentials can be tested. Of course, only the final a posteriori result gives a decisive information.

With a rough fit of the optimal functions, we ran two tests with Reynolds numbers used for the estimation of

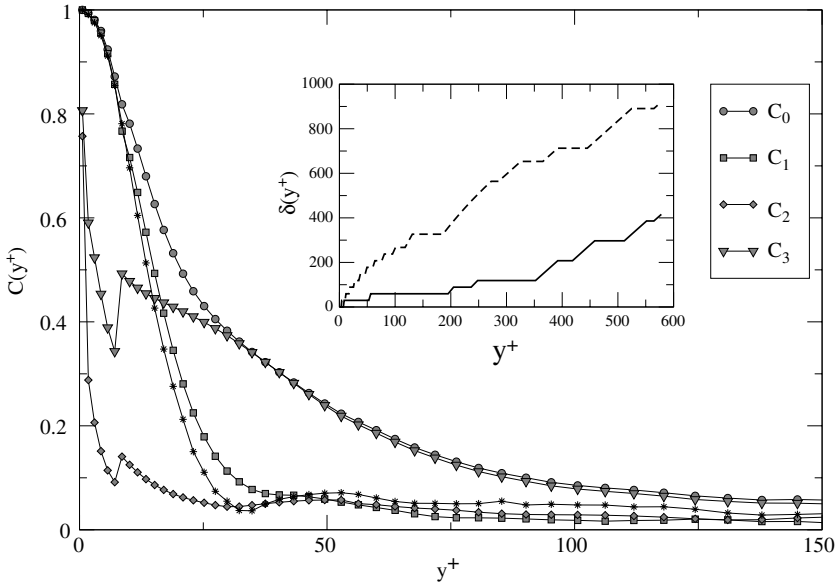

Fig. 6. Correlations C_0 (●), C_1 (■), C_2 (◊), and C_3 (▼) for the $\tau_{w,zy}$-component at $Re = 10{,}935$. The curve for Schumann's model is shown, too (*) corresponding to C_1. The inset shows the delay δ (straight line) in x^+ units, for comparison the graph for $\tau_{w,xy}$ is shown (dashed line).

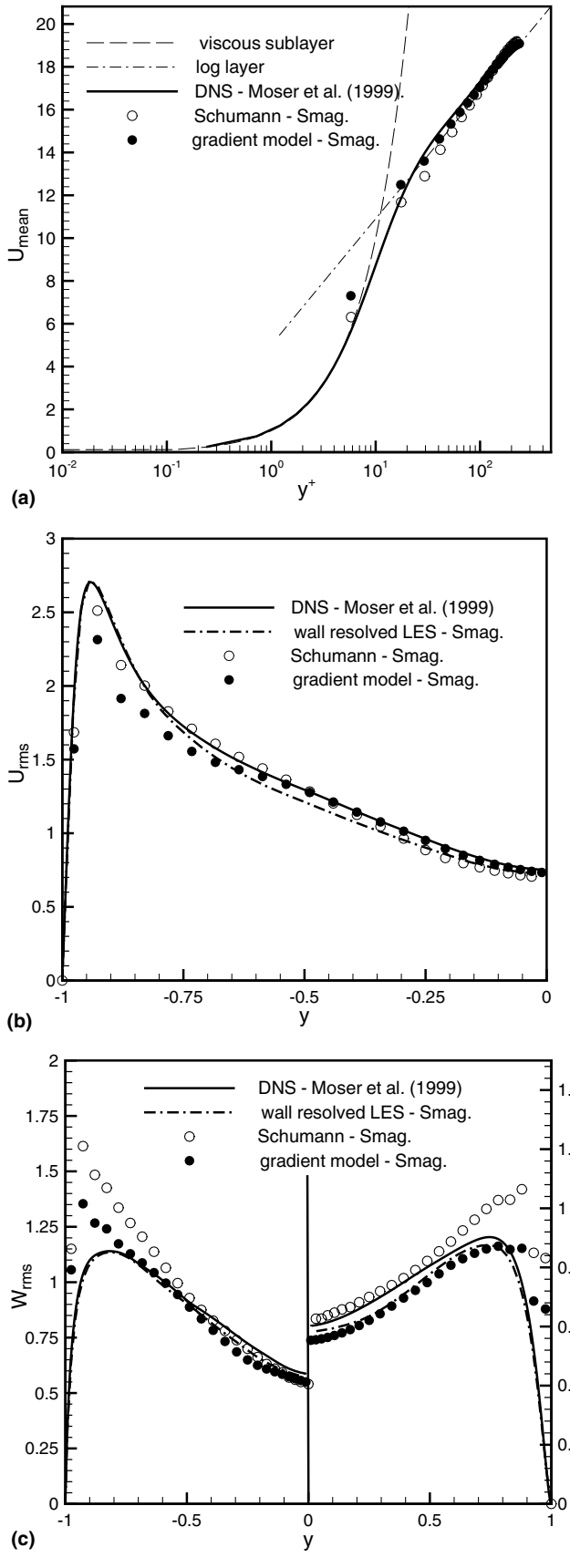

Fig. 7. Results on a posteriori LES for $\langle u(Y)\rangle$: (a) $u_{\mathrm{rms}}(Y)$, (b) $v_{\mathrm{rms}}(Y)$, and $w_{\mathrm{rms}}(Y)$ (c) at $Re = 10{,}935$; DNS data by Moser et al. (1999). The rms-values are normalized by the predicted wall shear stress velocities u_τ.

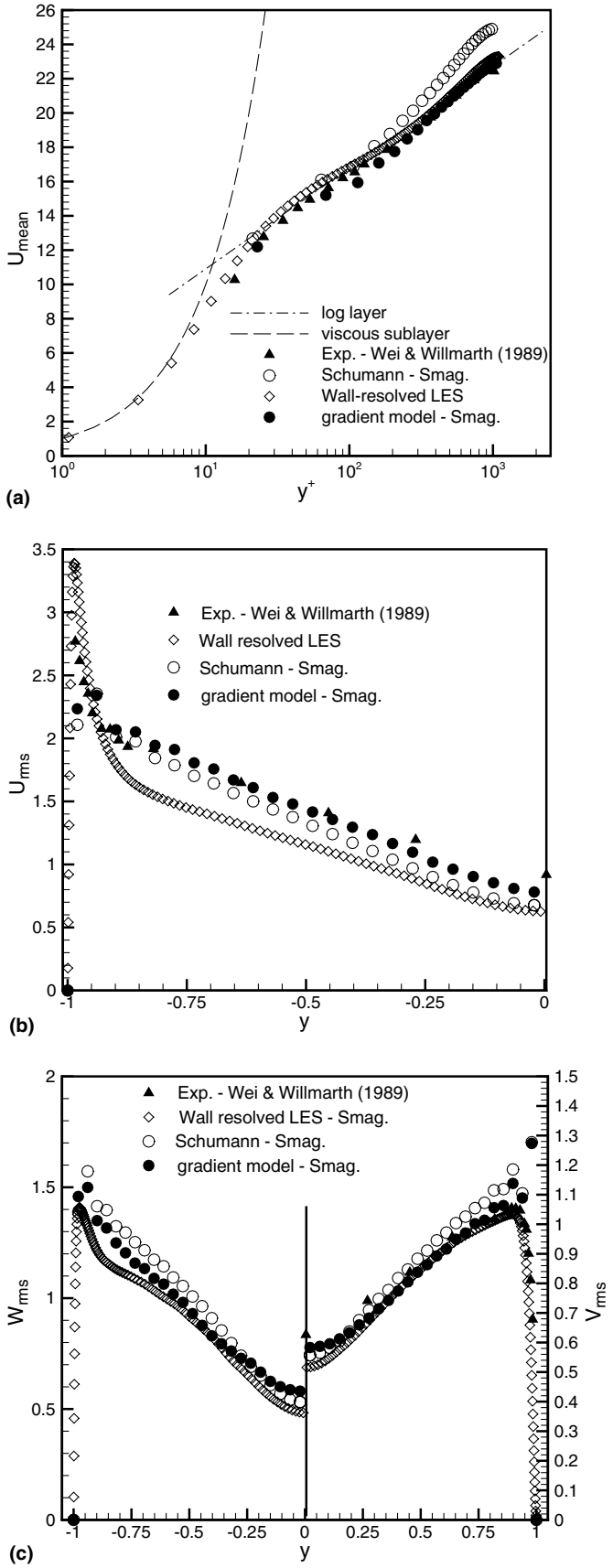

Fig. 8. Results on a posteriori LES for $\langle u(Y)\rangle$: (a) $u_{\mathrm{rms}}(Y)$, (b) $v_{\mathrm{rms}}(Y)$, and $w_{\mathrm{rms}}(Y)$ (c) at $Re = 22{,}776$, experimental data by Wei and Willmarth (1989) at $Re = 20{,}197$. The rms-values are normalized by the predicted wall shear stress velocities u_τ.

the models. We did not use higher Reynolds numbers in order to ensure consistency of the comparison. The first check has been set up with the first grid point at $y^+ = 5.8$, using the same x and z resolution as for the wall-resolved LES run at $Re = 10{,}935$. This way, a detailed comparison is possible. The second setup was at $Re = 22{,}776$ with the first grid point at $y^+ = 22.8$ in the buffer layer. It does not make sense to use larger distances, since the log-layer is of the order 10^2 for this Reynolds number. For comparison, we display results for $\langle u(Y)\rangle$, $u_{\mathrm{rms}}(Y)$, $v_{\mathrm{rms}}(Y)$, and $w_{\mathrm{rms}}(Y)$ of LES runs obtained with polynomial functions as approximations of the results. Note that the rms-values are normalized by the predicted wall shear stress velocities u_τ which are not fixed in the predictions but a result of the computation (fixed mass flow rate in the channel). We compare predictions of the gradient model with an LES prediction using Schumann's model, the wall-resolved LES used for NLSE, DNS data (Moser et al., 1999) ($Re = 10{,}935$), and experimental data (Wei and Willmarth, 1989) ($Re = 22{,}776$).

In Fig. 7(a)–(c) results for $Re = 10{,}935$ are shown. The average streamwise velocity agrees better with the DNS prediction than Schumann's model in the log-layer, only the first point is slightly overpredicted (Fig. 7(a)). For u_{rms}, we find a good coincidence with DNS and fully resolved LES in the bulk region and close to the wall; in between underprediction of the peak value is observed (Fig. 7(b)). The reason for these effects is an underestimation of the velocity gradient $\partial\overline{u}/\partial y$ by the gradient model in the LES prediction leading to a reduced turbulence production in this near-wall region. For v_{rms} and w_{rms} (Fig. 7(c)), our results are better than those of Schumann's model in the whole channel region.

The results for the second setup, $Re = 22{,}776$ are displayed in Fig. 8(a)–(c). From Fig. 8(a) we read that the average streamwise velocity agrees much better than Schumann's model with experimental and wall-resolved data. For u_{rms}, the difference between the models is not very large. For v_{rms} and w_{rms} (Fig. 8(c)), again the gradient model yields better coincidence with wall-resolved predictions and experimental measurements.

Summarizing this section, we have shown that NLSE yields models, usable straightforwardly from the output of the data analysis. We expect its main use in the case of complex geometries, especially for separating flows, where no models are known to capture the separation in a satisfying way.

5. Conclusions

In this paper, we present an approach to derive generalized additive wall models in nonparametric form using spatio-temporal data analysis. These wall models for LES are determined by estimating conditional expectation values. Based on the correlation of the model terms, the respective importance is determined.

- The pressure gradient model investigated is a generalization of existing models incorporating Schumann's model, Piomelli's shifted boundary condition and the ejection model. Additionally, fluctuating parts of the pressure gradient are included.
- In accordance with Piomelli et al. (1989), the shift of the boundary condition in streamwise direction substantially raises the correlation. As another result, it turns out that, in contrast to Piomelli et al. (1989), *sweeps* are correlating to the wall shear stress and not the ejection events.
- Our generalized model shows a significant contribution of the streamwise pressure gradient in the $\tau_{\mathrm{w},xy}$ component for a small range $y^+ < 10$; in the $\tau_{\mathrm{w},zy}$-component the spanwise pressure gradient dominates the dynamics. For an implementation into an LES prediction, the functions involved are given in parametrical form.
- The correlations between the wall shear stress and the near-wall velocity decrease with increasing wall distance. Because wall models for LES can only be applied if a correlation exists, wall functions in general are applicable to y^+ values of the order O(50) or smaller. This issue generally restricts the usefulness of any wall model. However, compared to the application of no-slip boundary conditions the resolution requirements and thus the computational costs of LES are strongly reduced.
- The dependence on the Reynolds number has been investigated by comparison of DNS and wall-resolved LES data for four different Reynolds numbers. A clear tendency can be observed, indicating convergence of the results.

To our knowledge it is the first time, the estimation of the full conditional statistics is carried out in the frame of wall modeling. The model is restricted to a generalized additive model, which is a common condition. Generalization to functions of several variables are possible but expensive due to the high dimensionality.

Acknowledgements

This work is part of the *Interdisciplinary Turbulence Initiative* and is supported by the *Deutsche Forschungsgemeinschaft* under contract numbers BR 1847/3 and PI 220/7. The DNS computations were carried out on the Fujitsu VPP 300 at the RRZE (Erlangen) and the Fujitsu VPP 700 at the Leibniz Computing Center (Munich), which are also gratefully acknowledged. Furthermore, M.A. acknowledges stimulating discussions with A. Pikovsky and R. Friedrich and thanks K. Ahnert for computer aid.

References

Abel, M., 2004. Nonparametric modeling and spatio-temporal data analysis. Int. J. Bifurcat. Chaos 14 (6), 2027.

Adrian, R.J., 1979. Conditional eddies in isotropic turbulence. Phys. Fluids 22 (11), 2065–2070.

Adrian, R.J., Jones, B.G., Chung, M.K., Hassan, Y., Nithianandan, C.K., Tung, A., 1989. Approximation of turbulent conditional averages by stochastic estimation. Phys. Fluids A 1, 992.

Balaras, E., Benocci, C., Piomelli, U., 1996. Two-layer approximate boundary conditions for large eddy simulations. AIAA J. 34 (6), 1111–1119.

Benzi, R., Amati, G., Casciola, G.M., Toschi, F., Piva, R., 2002. Intermittency and scaling laws for wall bounded turbulence. Phys. Fluids 11 (6), 1284–1286.

Breuer, M., 1998. Large eddy simulation of the sub-critical flow past a circular cylinder: numerical and modeling aspects. Int. J. Numer. Methods Fluids 28, 1281–1302.

Breuer, M., 2002. Direkte Numerische Simulation und Large-Eddy Simulation turbulenter Strömungen auf Hochleistungsrechnern. Habilitationsschrift, Universität Erlangen-Nürnberg, Berichte aus der Strömungstechnik, ISBN 3-8265-9958-6. Shaker Verlag, Aachen.

Buja, A., Hastie, T., Tibshirani, R., 1989. Linear smoothers and additive models. Ann. Stat. 17 (2), 453–555.

Craft, T.J., Gerasimov, A.V., Iacovides, H., Launder, B., 2002. Progress in the generalization of wall-function treatment. Int. J. Heat Fluid Flow 23, 148–160.

Ferziger, J.H., 1996. Large eddy simulation. In: Gatski, T., Hussaini, M., Lumley, J. (Eds.), Simulation and Modeling of Turbulent Flows. Oxford University Presss, Oxford, UK, pp. 109–154.

Ghosal, S., Moin, P., 1995. The basic equations of large eddy simulation of turbulent flows in complex geometry. J. Comput. Phys. 118, 24–37.

Green, P.J., Silverman, B.W., 1994. Nonparametric Regression and Generalized Linear Models. Chapman & Hall, London.

Grötzbach, G., 1987. Direct numerical and large eddy simulation of turbulent channel flow. In: Cheremisinoff, N. (Ed.), Encyclopedia of Fluid Mechanics, vol. 6. Gulf, West Orange, NJ, pp. 1337–1391.

Gualtieri, P., Casciola, G.M., Benzi, R., Amati, G., Piva, R., 2002. Scaling laws and intermittency in homogeneous shear flows. Phys. Fluids 14 (2), 583–596.

Hastie, T., Tibshirani, R., 1990. Generalized Additive Models. Chapman & Hall, London.

Hoffmann, G., Benocci, C., 1995. Approximate wall boundary conditions for large eddy simulations. In: Benzi, R. (Ed.), Advances in Turbulence. Kluwer, Berlin.

Honerkamp, J., 1994. Stochastic Dynamical Systems. VCH, New York.

Jimenèz, J., Siemens, M.P., 2001. Low-dimensional dynamics of a turbulent wall flow. J. Fluid Mech. 435, 81–91.

Langford, J., Moser, R.D., 1999. Optimal LES formulations for isotropic turbulence. J. Fluid Mech. 398, 321–346.

Meneveau, C., Katz, J., 2000. Scale-invariance and turbulence models for large eddy simulation. Ann. Rev. Fluid Mech. 32, 1–32.

Moin, P., 2002. Advances in large eddy simulation methodology for complex flows. Int. J. Heat Fluid Flow 23, 710–720.

Moser, R., Kim, J., Mansour, N., 1999. Direct numerical simulation of turbulent channel flow up to $Re_\tau = 590$. Phys. Fluids A 11 (4), 943–945.

Nicoud, F., Baggett, J.S., Moin, P., Cabot, W., 2001. Large eddy simulation wall-modeling based on suboptimal control theory and linear stochastic estimation. Phys. Fluids 13 (10), 2968–2984.

Piomelli, U., Balaras, E., 2002. Wall-layer models for large eddy simulations. Annu. Rev. Fluid Mech. 34, 349–374.

Piomelli, U., Ferziger, J., Moin, P., Kim, J., 1989. New approximate boundary conditions for large eddy simulations of wall-bounded flow. Phys. Fluids A 1, 1061–1068.

Pope, S.B., 2000. Turbulent Flows. Cambridge University Press, Cambridge, UK.

Rényi, A., 1959. On measures of dependence. Acta. Math. Acad. Sci. Hungary 10, 441–451.

Schumann, U., 1975. Subgrid-scale model for finite-difference simulations of turbulent flows in plane channels and annuli. J. Comput. Phys. 18, 376–404.

Silverman, B.W., 1996. Density Estimation for Statistics and Data Analysis. Chapman & Hall, London.

Teukolsky, S.A., Vetterling, W.T., Flannery, B.P., 1993. Numerical Recipes in C: The Art of Scientific Computing, second ed. Cambridge University Press, Cambridge.

Toschi, F., Amati, G., Succi, S., Benzi, R., Piva, R., 1999. Intermittency and structure functions in channel flow turbulence. Phys. Rev. Lett. 82, 5044.

Vasilyev, O., Lund, T., Moin, P., 1998. A general class of commutative filters for LES in complex geometries. J. Comput. Phys. 146, 82–104.

Völker, S., Moser, R.D., Venugopal, P., 2002. Optimal large eddy simulation of turbulent channel flow based on direct numerical simulation data. Phys. Fluids 14 (10), 3675–3691.

Voss, H.U., Buenner, M., Abel, M., 1998. Identification of continuous spatio-temporal systems. Phys. Rev. E 57 (3), 2820–2823.

Wei, T., Willmarth, W.W., 1989. Reynolds-number effects on the structure of a turbulent channel flow. J. Fluid Mech. 204, 57–95.

Werner, H., Wengle, H., 1993. Large eddy simulation of turbulent flow over and around a cube in a plate channel. In: 8th Symp. on Turb. Shear Flows. Springer-Verlag, Berlin, pp. 155–168.